Proceedings of DETC2001
2001 ASME Design Engineering Technical Conferences
September 9-13, 2001, Pittsburgh, Pennsylvania, USA

DETC2001/VIB-21438

DYNAMICS OF TOWED CABLES DURING TRANSIENT MOTIONS

Leslie Ng
Dept. of Theoret. & Appl. Mechanics
Cornell University, Ithaca, NY 14853
email:lhn2@cornell.edu

Richard Rand
Dept. of Theoret. & Appl. Mechanics
Cornell University, Ithaca, NY 14853
email:rhr2@cornell.edu

William Keith
Naval Undersea Warfare Center
Newport, RI 02841
email:wlkeith@hotmail.com

ABSTRACT

This work concerns the problem of determining the relative position of a towed cable when the towing vessel is moving in an arbitrary given fashion. In particular we are concerned with avoiding the tangling of individual towed cables when the towing vessel is towing multiple cables. A model is developed to describe the dynamics of the tow cables for arbitrary motions of the towing vessel. The model is then analyzed for constant speed circular motions of the towing vessel. A combination of analytic and numerical techniques are used in the analysis of the resulting differential equations.

INTRODUCTION

Ships often tow cables for a variety of applications such as acoustic sensing, cable laying and scientific experiments. We investigate the dynamics of towed cables during transient motions of the towing vessel. In particular, we are interested in avoiding the tangling of individual towed cables when multiple cables are towed.

When multiple cables are towed by a vessel, individual tow lines are kept separated by the use of small lifting devices, referred to as 'lateral force devices' or LFDs. An LFD is designed so that if the towing vessel is moving in a straight line S at constant speed, the tow line joining the LFD to the vessel will make an constant angle α with S in steady-state. In steady-state, the fluid force generated by the LFD $\overline{F}$ and the tension $\overline{T}$ of the tow cable on the LFD sum to zero. Fig.1 illustrates the steady-state motion of the LFD for constant velocity motion of the vessel.

In this work we develop a simple two dimensional model for an LFD being towed by a vessel moving in an arbitrary motion. We then investigate the model for the special case where the vessel is moving in a circle at constant speed and discuss some of the limitations of the model. The AUTO bifurcation and continuation software package is used to numerically generate bifurcation diagrams. For the analytic calculations, the computer algebra program Macsyma is used extensively. Finally, we present some physical applications for the model developed.

TWO DIMENSIONAL MODEL

In our model, we treat the LFD as a point mass and the tow cable as inextensible. Considering only motion in a horizontal plane, let (x, y) describe the position of the LFD and (f, g) describe the position of the towing vessel. Fig.2 shows the forces acting on the LFD. We assume that the angle between the force $\overline{F}$ of the fluid on the LFD and the velocity vector of the LFD remains α, even when the system is not in steady state. Using Newton's laws, the equations of motion for the LFD have the form:

$$m\ddot{x} = -T_x + F_x, \quad m\ddot{y} = -T_y + F_y \tag{1}$$

where, m is the mass of the LFD and (T_x, T_y) and (F_x, F_y) are the (x, y) components of $\overline{T}$ and $\overline{F}$ respectively. Because we treat the cable as inextensible, we have the constraint:

$$(x - f)^2 + (y - g)^2 = L^2 \tag{2}$$

Using the constraint, T_x and T_y can be expressed as:

$$T_x = T\frac{x - f}{L}, \quad T_y = T\frac{y - g}{L} \tag{3}$$

where, $T = |\overline{T}|$. From Fig.2 we can see that:

$$F_x = F\cos(\beta + \alpha) \tag{4}$$
$$F_y = F\sin(\beta + \alpha) \tag{5}$$

where, $F = |\overline{F}|$. Eqs.(4),(5) can be written:

$$F_x = F\cos\alpha\cos\beta - F\sin\alpha\sin\beta \tag{6}$$
$$F_y = F\cos\alpha\sin\beta + F\sin\alpha\cos\beta \tag{7}$$

In our model, we take the magnitude of the fluid force to be proportional to the square of the speed of the LFD v.

$$F = kv^2 = k(\dot{x}^2 + \dot{y}^2) \tag{8}$$

where, k is a fluid force constant. We also assume the angle α to be independent of the velocity of the LFD. Using Eq.(8) and since $\sin\beta = -\frac{\dot{y}}{\sqrt{\dot{x}^2+\dot{y}^2}}$ and $\cos\beta = -\frac{\dot{x}}{\sqrt{\dot{x}^2+\dot{y}^2}}$, Eqs. (6),(7) become:

$$F_x = k\sqrt{\dot{x}^2 + \dot{y}^2}(-\dot{x}\cos\alpha + \dot{y}\sin\alpha) \tag{9}$$
$$F_y = k\sqrt{\dot{x}^2 + \dot{y}^2}(-\dot{y}\cos\alpha - \dot{x}\sin\alpha) \tag{10}$$

Combining Eqs.(1),(3),(9),(10) we arrive at the following equations governing the motion of the LFD:

$$m\ddot{x} + \frac{T}{L}(x - f) = k\sqrt{\dot{x}^2 + \dot{y}^2}(-\dot{x}\cos\alpha + \dot{y}\sin\alpha) \tag{11}$$
$$m\ddot{y} + \frac{T}{L}(y - g) = k\sqrt{\dot{x}^2 + \dot{y}^2}(-\dot{y}\cos\alpha - \dot{x}\sin\alpha) \tag{12}$$

Thus, we have a 2 degree of freedom system subject to the constraint Eq.(2) with T being the magnitude of the constraint force. Eqs.(11),(12) can be combined by eliminating T and using the constraint Eq.(2) to form a single equation. We start by defining an angle θ as the angle the LFD cable makes with the y axis as show in Fig.3.

Substituting $x = f + L\sin\theta$ and $y = g - L\cos\theta$ into Eqs.(11),(12), eliminating T and solving for $\ddot{\theta}$ gives:

$$\ddot{\theta} = -\frac{1}{L}\Big[\ \ddot{g}\sin\theta + \ddot{f}\cos\theta + \frac{k}{m}\sqrt{\begin{matrix}L^2\dot{\theta}^2 + \dot{g}^2 + \dot{f}^2 \\ +2L(\dot{g}\sin\theta + \dot{f}\cos\theta)\dot{\theta}\end{matrix}} \times \Big(\dot{\theta}L\cos\alpha + (\dot{f}\sin\alpha + \dot{g}\cos\alpha)\sin\theta + (\dot{f}\cos\alpha - \dot{g}\sin\alpha)\cos\theta\Big)\ \Big] \tag{13}$$

We are left with a single equation on θ involving the functions f and g and their derivatives which specify the motion of the towing vessel.

CIRCULAR MOTIONS OF THE TOWING VESSEL

For the special case in which the towing vessel moves in a circle at constant speed we set $f = R\cos\omega t$ and $g = R\sin\omega t$, R being the turning radius and ω the angular frequency. Substituting these into Eq.(13) results in an equation involving t. If we define a new angle ϕ such that $\theta = \omega t + \phi$ we can greatly simplify the equations of motion. We can think of a physical interpretation of ϕ as the angle the LFD cable makes with the instantaneous velocity of the towing vessel. Fig.4 shows the angle ϕ. Substituting $f = R\cos\omega t$, $g = R\sin\omega t$ and $\theta = \omega t + \phi$ into Eq.(13) and solving for $\ddot{\phi}$, we get:

$$\ddot{\phi} = -\frac{1}{L}\Big[\ \frac{k}{m}\sqrt{\begin{matrix}(R^2 + 2LR\sin\phi + L^2)\omega^2 + \dot{\phi}^2L^2 \\ +2(\dot{\phi}LR\sin\phi + \dot{\phi}L^2)\omega\end{matrix}} \times \Big(\dot{\phi}L\cos\alpha + ((\cos\alpha\sin\phi - \sin\alpha\cos\phi)R + L\cos\alpha)\omega\Big) - R\omega^2\cos\phi\ \Big] \tag{14}$$

Using the angle ϕ as the coordinate, we have transformed the nonautonomous equation into an autonomous one. Finally we can eliminate some of the parameters by nondimensionalizing the system. Rescaling $\hat{k} = \frac{k}{mL}$, $\hat{R} = \frac{R}{L}$, $\hat{t} = \omega t$ and dropping the hats gives:

$$\ddot{\phi} = -k\sqrt{(R^2 + 2R\sin\phi + 1) + 2(\dot{\phi}R\sin\phi + \dot{\phi}) + \dot{\phi}^2} \times \Big(\dot{\phi}\cos\alpha + ((\cos\alpha\sin\phi - \sin\alpha\cos\phi)R + \cos\alpha)\Big) + R\cos\phi \tag{15}$$

The rescaling has the same effect as setting $m = L = \omega = 1$ in Eq.(14). We are now left with a second order autonomous differential equation with 3 parameters k, R and α.

LIMITATIONS OF THE MODEL

In our model we have assumed the cable is inextensible and exerts a constraint force T on the LFD. This is only valid for positive values of T where the cable is in tension. The cable should not be allowed to support compressive loads resulting in a negative values of T. When T becomes negative we should remove the length constraint omitting any constraint force. Also, if the cable is not in tension the LFD may not align itself properly, which would be undesirable. Thus in our previous model we should only consider

motions where T remains positive. We can solve for the constraint force T to get:

$$T = k\sqrt{\begin{matrix}(R^2 + 2LR\sin\phi + L^2)\omega^2 + \dot{\phi}^2L^2 \\ +2(\dot{\phi}LR\sin\phi + \dot{\phi}L^2)\omega\end{matrix}} \times \quad (16)$$
$$\Big(\dot{\phi}L\sin\alpha + ((\sin\alpha\sin\phi + \cos\alpha\cos\phi)R + L\sin\alpha)\omega \Big)$$
$$+ (mR\sin\phi + mL)\omega^2 + 2m\dot{\phi}L\omega + m\dot{\phi}^2L$$

Also, note that the parameter α represents the angle the fluid force makes with the velocity vector of the LFD. Physically, we are restricted to $|\alpha| \leq \frac{\pi}{2}$ because having $|\alpha| \geq \frac{\pi}{2}$ would mean the LFD generates a fluid force with a component in the direction of its velocity vector which is unrealizable. At the critical values $\alpha = \pm\frac{\pi}{2}$ the model breaks down.

It is interesting to note that when $\alpha = \pm\frac{\pi}{2}$, the system has a reversible symmetry and the system is integrable. Taking $(\phi \mp \frac{\pi}{2}, t) \rightarrow (-(\phi \mp \frac{\pi}{2}), -t)$ results in the same equation. In the $\phi, \dot{\phi}$ phase plane, trajectories starting on the line $\phi = \pm\frac{\pi}{2}$ follow symmetric paths backwards and forwards in time. If the trajectories reintersect the line $\phi = \pm\frac{\pi}{2}$ they form closed curves.

AUTO ANALYSIS

The AUTO bifurcation and continuation software package (Doedel et al., 1998) was used to numerically obtain curves for saddle-node, Hopf and homoclinic bifurcations in Eq.(15). For fixed values of k, we generate plots for the bifurcation curves in R and α.

The bifurcation diagram generated for $k = 1$ is shown in Fig.5. We see that there exists a variety of dynamical features particularly around the region $\alpha = -\frac{\pi}{2}$. Numerical integrations show that there are no fixed points in the regions bounded by the $R = 0$ axis and the saddle-node bifurcation curves that extend from $R = 0$, $\alpha = -\frac{\pi}{2}$ to $R = 0$, $\alpha = \frac{\pi}{2}$. In the 'arrow-head' shaped region around $\alpha = -\frac{\pi}{2}$ that is bounded by the saddle-node bifurcation curves there are 4 fixed points and in the remaining regions there are 2 fixed points. Several cusps are present where 2 saddle-node bifurcation curves come together and there also appears to be a pair of Takens-Bogdanov bifurcation points where the saddle-node, Hopf and homoclinic bifurcations all meet.

For different values of k, the bifurcation diagrams generated are similar to the one obtained for $k = 1$. For general k, the majority of the dynamical features appear to be centered around the line $\alpha = -\frac{\pi}{2}$. The main features appear to be an 'arrow-head' shaped curve of saddle-node bifurcations centered around $\alpha = -\frac{\pi}{2}$, curves of homoclinic bifurcations which lie inside this 'arrow-head' region, a curve of Hopf bifurcations which partly lies above and extends into the 'arrow-head' region and a curve of saddle-node bifurcations which extends from $\alpha = \frac{\pi}{2}$ to $\alpha = -\frac{\pi}{2}$.

BIFURCATION ANALYSIS

The analysis of nonlinear systems starts with determining the equilibrium points of the system. Equilibrium points for Eq.(15) occur when $\dot{\phi} = 0$ and $\phi = const = \phi^*$. Substituting this into Eq.(15), we obtain the following condition for equilibrium points of the system:

$$k\sqrt{R^2 + 2R\sin\phi^* + 1} \times \quad (17)$$
$$\Big((-\cos\alpha\sin\phi^* + \sin\alpha\cos\phi^*)R - \cos\alpha\Big) + R\cos\phi^* = 0$$

To determine the stability of the equilibrium points, we look at their linearizations. Setting $\phi = \phi^* + \epsilon\xi$ in Eq.(15) and Taylor expanding in ϵ, we obtain an eigenvalue equation of the form:

$$\lambda^2 + B\lambda + C = 0 \quad (18)$$

where,

$$B = \frac{k}{\sqrt{G}}\Big((\cos\alpha\sin^2\phi^* - \sin\alpha\cos\phi^*\sin\phi^* + \cos\alpha)R^2 \quad (19)$$
$$+ (4\cos\alpha\sin\phi^* - \sin\alpha\cos\phi^*)R + 2\cos\alpha\Big)$$
$$C = \frac{kR}{\sqrt{G}}\Big((\sin\alpha\sin\phi^* + \cos\alpha\cos\phi^*)R^2 \quad (20)$$
$$+ (3\sin\alpha\sin^2\phi^* + 3\cos\alpha\cos\phi^*\sin\phi^* - \sin\alpha)R$$
$$+ \sin\alpha\sin\phi^* + 2\cos\alpha\cos\phi^*\Big) + R\sin\phi^*$$
$$G = R^2 + 2R\sin\phi^* + 1$$

Using Eqs.(17),(19),(20), we perform a bifurcation analysis of the equilibria. The following analysis relies heavily on the computer algebra software package Macsyma.

The condition that the system undergoes a saddle-node bifurcation is that an equilibrium point has a zero eigenvalue. This occurs when $C = 0$ in Eq.(18). Note that an equivalent condition is that there is a double root in ϕ^* in Eq.(17). This is represented by taking the partial derivative of Eq.(17) by ϕ^*. It can be shown that these two conditions result in equivalent expressions. Thus we have 2 equations (the equation for equilibrium points and the $C = 0$ equation) and 4 unknowns (k, R, α and ϕ^*). Combining these 2

equations we can eliminate ϕ^* to produce a single equation for the saddle-node bifurcation curve involving only k, R and α. The resulting equation for saddle-node bifurcation curves has 120 terms (omitted for brevity).

The condition for Hopf bifurcations is that an equilibrium point has purely imaginary eigenvalues. This occurs when $B = 0$ in Eq.(18). Again we have 2 equations and 4 unknowns which can be combined to produce a single equation in k, R and α for Hopf Bifurcations. The expression for the Hopf bifurcation curve has 30 terms (again, omitted for brevity).

For $k = 1$, these equations correspond with the numerical results obtained using AUTO. Using Macsyma, we can create implicit plots for the analytic expressions for saddle-node and Hopf Bifurcations. Fig.6 shows a plot of the expressions for the saddle-node and Hopf bifurcations for $k = 1$. We see from Fig.6 that the analytic expressions check with the numerical results obtained previously using AUTO (see Fig.5) but there are also additional features present. The dotted lines in Fig.6 correspond to parts of the curves that were not present in the AUTO analysis. Both bifurcation curves have their mirror image repeated $\alpha = \frac{\pi}{2}$. Also, the Hopf bifurcation has a segment which continues below the Takens-Bogdanov points.

Numerical integration shows that these additional features do not really exist but rather are spurious artifacts of the computation.

INTERSECTION OF HOPF AND HOMOCLINIC BIFURCATION CURVES

In the bifurcation diagrams obtained using AUTO, we see that the Hopf and homoclinic bifurcation curves intersect. Further investigation around the region where the curves cross reveals there exists a curve of saddle-node bifurcation of periodic orbits and that the Hopf bifurcation changes from supercritical to subcritical. Curves of saddle-node bifurcations of periodic orbits typically terminate at degenerate Hopf and trace 0 saddle-loop (homoclinic) bifurcations (Guckenheimer, 1986). Fig.7 shows the phase portraits near the region $R \approx 1.5$, $\alpha \approx -1.4$ where the Hopf and homoclinic curves cross for the $k = 1$ bifurcation diagram. See (Hubbard and West, 1995), p.331, for a discussion of this bifurcation.

At the degenerate Hopf bifurcation, the Hopf bifurcation changes from supercritical to subcritical. Determining whether a Hopf bifurcation is supercritical or subcritical involves looking at the normal form. In polar coordinates, the normal form of the Taylor series of degree 3 for the Hopf bifurcation is:

$$\dot{r} = (d\mu + \sigma r^2)r \tag{21}$$

$$\dot{\theta} = (w + c\mu + br^2)$$

The sign of the cubic coefficient σ in the $\dot{r}$ equation determines whether the Hopf bifurcation is supercritical or subcritical. At the degenerate Hopf bifurcation, we have $\sigma = 0$. For more details see (Guckenheimer and Holmes, 1983). For our calculations, we use an alternative form for this condition obtained by Andronov for a general planar analytic system with Taylor series (Perko, 1996):

$$\begin{aligned}\dot{x} &= a_{10}x + a_{01}y + a_{20}x^2 + a_{11}xy + a_{02}y^2 \\ &\quad + a_{30}x^3 + a_{21}x^2y + a_{12}xy^2 + a_{03}y^3 + \ldots \\ \dot{y} &= b_{10}x + b_{01}y + b_{20}x^2 + b_{11}xy + b_{02}y^2 \\ &\quad + b_{30}x^3 + b_{21}x^2y + b_{12}xy^2 + b_{03}y^3 + \ldots\end{aligned} \tag{22}$$

The condition for a degenerate Hopf is $\sigma = 0$, where

$$\begin{aligned}\sigma = \frac{-3\pi}{2a_{01}\Delta^{3/2}}\Big(&[a_{10}b_{10}(a_{11}^2 + a_{11}b_{02} + a_{02}b_{11}) \\ &+ a_{10}a_{01}(b_{11}^2 + a_{20}b_{11} + a_{11}b_{02}) \\ &+ b_{10}^2(a_{11}a_{02} + 2a_{02}b_{02}) - 2a_{10}b_{10}(b_{02}^2 - a_{20}a_{02}) \\ &- 2a_{10}a_{01}(a_{20}^2 - b_{20}b_{02}) - a_{01}^2(2a_{20}b_{20} + b_{11}b_{20}) \\ &+ (a_{01}b_{10} - 2a_{10}^2)(b_{11}b_{02} - a_{11}a_{20})] \\ -(a_{10}^2 + a_{01}b_{10})&[3(b_{10}b_{03} - a_{01}a_{30}) + 2a_{10}(a_{21} + b_{12}) \\ &+ (b_{10}a_{12} - a_{01}b_{21})]\Big)\end{aligned} \tag{23}$$

where $\Delta = a_{10}b_{01} - a_{01}b_{10}$. To obtain an expression for the degenerate Hopf bifurcation point, we start by writing Eq.(15) as a system of two first order ODE's with $\phi = w, \dot{\phi} = z$:

$$\begin{aligned}\dot{w} &= z \\ \dot{z} &= -k\sqrt{(R^2 + 2R\sin w + 1) + (2R\sin w + 2)z + z^2} \times \\ &\quad \Big(z\cos\alpha + (\cos\alpha\sin w - \sin\alpha\cos w)R + \cos\alpha\Big) \\ &\quad + R\cos w\end{aligned} \tag{24}$$

Taylor expanding around the equilibrium points located at $w = \phi = \phi^*, z = \dot{\phi} = 0$ we obtain:

$$\begin{aligned}\dot{w} &= z \\ \dot{z} &= b_{00} + b_{10}w + b_{01}z + b_{20}w^2 + b_{11}wz + b_{02}z^2 + b_{30}w^3 \\ &\quad + b_{21}w^2z + b_{12}wz^2 + b_{03}z^3 + \ldots\end{aligned} \tag{25}$$

Note that $b_{00} = 0$ because we are at an equilibrium point and $b_{01} = 0$ because we are on the Hopf bifurcation curve.

Also, $a_{01} = 1$ and all other $a_{ij} = 0$. Our condition for the degenerate Hopf bifurcation $\sigma = 0$ reduces to:

$$\sigma = -b_{11}b_{20} + b_{10}b_{11}b_{02} - b_{10}(3(b_{10}b_{03}) - b_{21}) = 0 \quad (26)$$

The remaining b_{ij} are functions of R, k, α and ϕ^*. Combining the equilibrium point equation, the expression previously obtained for the Hopf bifurcation curve and the equation $\sigma = 0$, we obtain a polynomial in R and k which contains 37 terms for the degenerate Hopf bifurcation point.

For a given value of k the polynomial can be solved numerically for R. One of the roots of the polynomial corresponds to value of R where the degenerate Hopf bifurcation occurs. Values for α can be obtained by substituting the value of R back into the expression for the Hopf bifurcation curve. The following table compares the value of R obtained by solving the polynomial for different values of k and with the data obtained using AUTO for the degenerate Hopf bifurcation.

k	R from AUTO	R from expression
0.5	2.454374	2.45457
1	1.585319	1.58535
1.5	1.324478	1.32449
2	1.207344	1.20735
3	1.105772	1.10578

Note that the values obtained from AUTO are slightly lower than the analytic values. This is due to the fact that AUTO can only get so close to the degenerate Hopf with its continuation routines.

PHYSICAL APPLICATIONS

Here we present some physical applications for the model developed.

A basic question is whether or not there exists stable circular motion for the LFD. This corresponds to whether there are stable equilibrium points in Eq.(15). Recall that our model is only valid if the tow cable remains in tension. We can see that for equilibria located at $|\phi^*| \geq \frac{\pi}{2}$ the cable will have to support compressive loads because the LFD would be leading the towing vessel. Thus, we are only concerned with changes of stability for equilibrium points with $|\phi^*| \leq \frac{\pi}{2}$. Also note we only need to consider values of $|\alpha| \leq \frac{\pi}{2}$ because only these values are physically realizable.

Numerical integration shows that the stability of equilibria located at $|\phi^*| \leq \frac{\pi}{2}$ are affected only by (i) the segment of the saddle-node bifurcation curve emanating from $R = 0$, $\alpha = \frac{\pi}{2}$ that extends to $\alpha = -\frac{\pi}{2}$ and by (ii) the upper portion of the Hopf bifurcation curve (see Fig.5). Fig.8 illustrates two situations where crossing these bifurcation curves affects the stability of equilibria for $k = 1$. The bifurcations associated with the other parts of the bifurcation curves involve equilibria with $|\phi^*| \geq \frac{\pi}{2}$.

To determine the minimum turning radius where an LFD has a stable circular motion we consider fixed values of k and α and let R vary. Numerics show that for large R, we are above the previously mentioned bifurcation curves and there exists a single stable equilibrium point located at $|\phi^*| \leq \frac{\pi}{2}$. As R decreases there is a critical value where the stability of the equilibrium point changes. There are two possible ways that the stability can change. Either a Hopf bifurcation occurs as shown by the path with points A, B, C in Fig.8 or a saddle-node bifurcation occurs as shown by the path with points D, E, F in Fig.8.

If a saddle-node bifurcation occurs there is no longer a stable circular motion for the LFD. Trajectories in the $\phi, \dot{\phi}$ phase space become unbounded which physically corresponds to motions where the cable is no longer in tension. If a Hopf bifurcation occurs, a stable limit cycle is created so that the LFD starts to oscillate. The oscillation initially grows as the turning radius of the towing vessel decreases.

To determine which of these two possibilities will occur we must calculate the value of $\alpha = \alpha_c$ where the Hopf bifurcation curve has a vertical tangent (see Fig.8). For values of $\alpha \leq \alpha_c$ a Hopf bifurcation occurs first, otherwise a saddle-node bifurcation occurs. To obtain α_c we set to zero the partial derivative with respect to R of the expression for the Hopf bifurcation. Combining this equation with the Hopf bifurcation expression, we can eliminate R to get a single equation on α which we can solve to get the value of α_c as a function of k. Using Macsyma, we find that $\cos\alpha_c = \frac{1}{3}$ (independent of k), that is $\alpha_c = -\cos^{-1}(\frac{1}{3}) \approx -1.231$. This value is consistent with the results obtained using AUTO.

If we further decrease R after a Hopf bifurcation occurs, several things can happen to the stable limit cycle thus created. The limit cycle may grow in amplitude and then shrink back down into a second Hopf bifurcation as shown by points A, B, C in Fig.8. At point C in Fig.8 we are back to a stable equilibrium point which is destroyed later in a saddle-node bifurcation if R is further decreased. Here we have two different ranges of R where a stable equilibria exists separated by a region where there are oscillatory motions. For values of α closer to $\alpha = -\frac{\pi}{2}$, as the limit cycle grows in size, it may be destroyed if we cross the homoclinic bifurcation curve or the saddle-node bifurcation of cycles curve. However, as R is further decreased,

we have a stable equilibrium point again after we cross the lower portion of the Hopf bifurcation curve. The analysis for the degenerate Hopf bifurcation point allows us to determine whether the equilibria becomes stable again due to a supercritical or subcritical Hopf bifurcation.

In all of these cases, we must also remember that the model is only valid when the cable is in tension. As the amplitude of the limit cycle grows, it is more likely that the cable is no longer in tension for the entire cycle.

Finally, we consider the case where a vessel is towing multiple cables which are being kept from tangling with one another through the use of LFD's. The model developed can be used to determine if the lines will tangle during turning. Consider the case of two different tow lines represented by $\varrho_1, m_1, k_1, L_1, \alpha_1$ and $\phi_2, m_2, k_2, L_2, \alpha_2$ respectively. The equations for equilibrium points are:

$$\frac{k_1}{m_1}\sqrt{R^2 + 2L_1 R\sin\phi_1^* + L_1^2}\times \left((\cos\alpha_1\sin\phi_1^* - \sin\alpha_1\cos\phi_1^*)R + L_1\cos\alpha_1\right) - R\cos\phi_1^* = 0 \tag{27}$$

$$\frac{k_2}{m_2}\sqrt{R^2 + 2L_2 R\sin\phi_2^* + L_2^2}\times \left((\cos\alpha_2\sin\phi_2^* - \sin\alpha_2\cos\phi_2^*)R + L_2\cos\alpha_2\right) - R\cos\phi_2^* = 0 \tag{28}$$

If $\phi_1^* = \phi_2^* = \phi^*$ the tow lines will tangle. We can eliminate ϕ^* and combine Eqs.(27),(28) into a single equation which is the condition for tangling. For given values of m_1, k_1, L_1, α_1, m_2, k_2, L_2 and α_2 we can solve the equation for R which gives us the turning radius where tangle occurs.

CONCLUSIONS

We have developed a 2-D model describing the motion of an LFD being towed by a vessel moving in an arbitrary fashion. For the special case where the vessel moves in a circle at constant speed we have found that the equations of motion can be reduced to a second order autonomous differential equation.

The analysis of the differential equations describing the motion of the LFD when the towing vessel moves in a circle at constant speed shows that the system has a complicated bifurcation structure. Analytic expressions were obtained for saddle-node and Hopf bifurcations.

Several physical applications for the model developed are presented. The model allows us to predict (i) the minimum turning radius of the towing vessel such that the LFD has a stable circular motion, (ii) parameters for which the LFD exhibits oscillatory behavior, and (iii) whether, for given parameters, two different tow lines will tangle.

Future work may include modifying the model taking into account that the cable is not able to support compressive loads. Also, a different form for the fluid force exerted by the LFD may be used. Finally, the model could be analyzed for different motions of the towing vessel.

ACKNOWLEDGEMENTS

The authors thank Professor John Guckenheimer of Cornell University for his help on the bifurcations encountered and Professor Paul Steen of Cornell University for his help in the use of the AUTO software. This work was partially supported by the Natural Sciences and Engineering Research Council of Canada (NSERC) and by the Office of Naval Research, Program Officer Dr. Roy Elswick, Code 321.

REFERENCES

Doedel, E., Champneys, A., Fairgrieve, T., Kuznetsov, Y., Sandstede, B., Wang, X., *AUTO 97: Continuation and Bifurcation Software for Ordinary Differential Equations*, 1998.

Guckenheimer, J. and Holmes, P., *Nonlinear Oscillators, Dynamical Systems, and Bifurcations of Vector Fields*, Springer-Verlag, 1983.

Guckenheimer, J., *Multiple Bifurcations Problems for Chemical Reactors*, Physica 20D (1986), pp.1-20.

Hubbard, J. H. and West, B. H., *Differential Equations: A Dynamical Systems Approach*, Springer-Verlag, 1995.

Perko, L., *Differential Equations and Dynamical Systems*, Springer-Verlag, 1996.

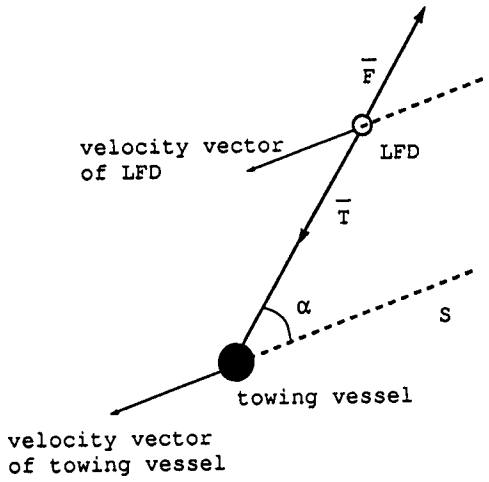

Fig.1. Steady-state motion of LFD resulting from constant velocity motion of towing vessel. All motion takes place in a horizontal plane.

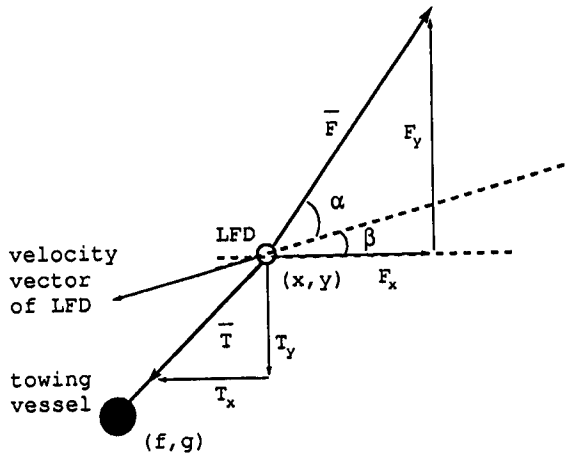

Fig.2. Free body diagram of LFD. View is looking down on a horizontal plane.

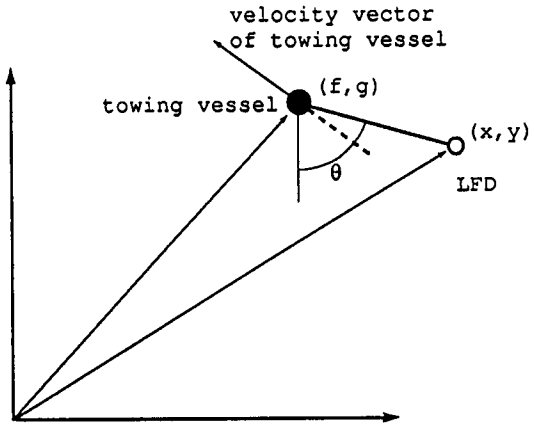

Fig.3. Angle θ defined.

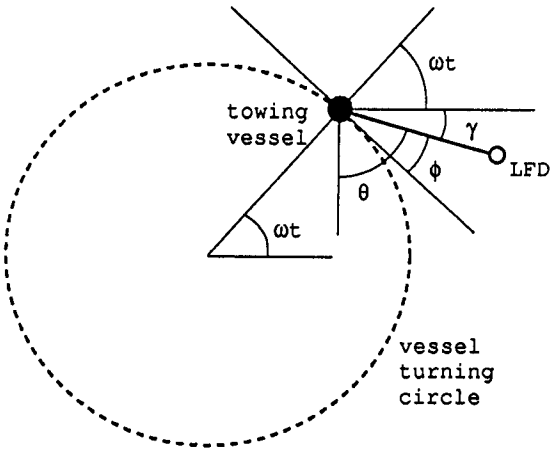

Fig.4. Angle ϕ defined. We have $\phi + \gamma + \omega t = \pi/2$ and $\gamma + \theta = \pi/2$ which gives $\theta = \omega t + \phi$.

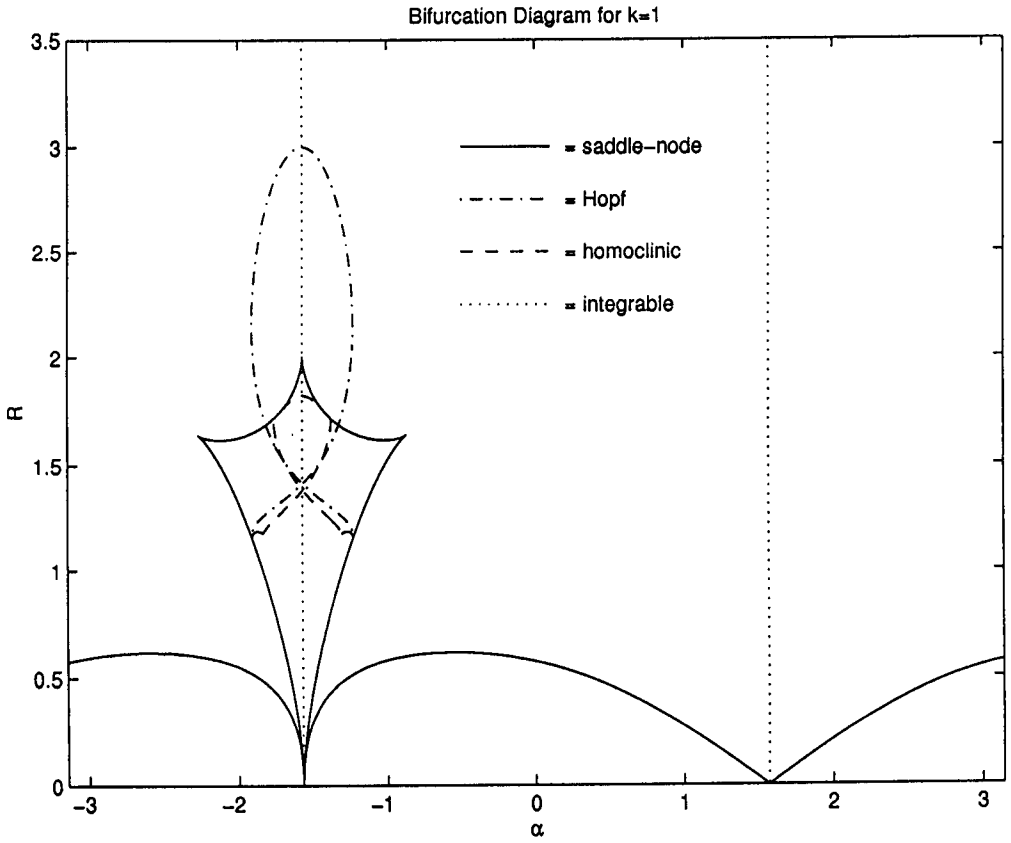

Fig.5. Bifurcation diagram for $k = 1$, as obtained by using AUTO.

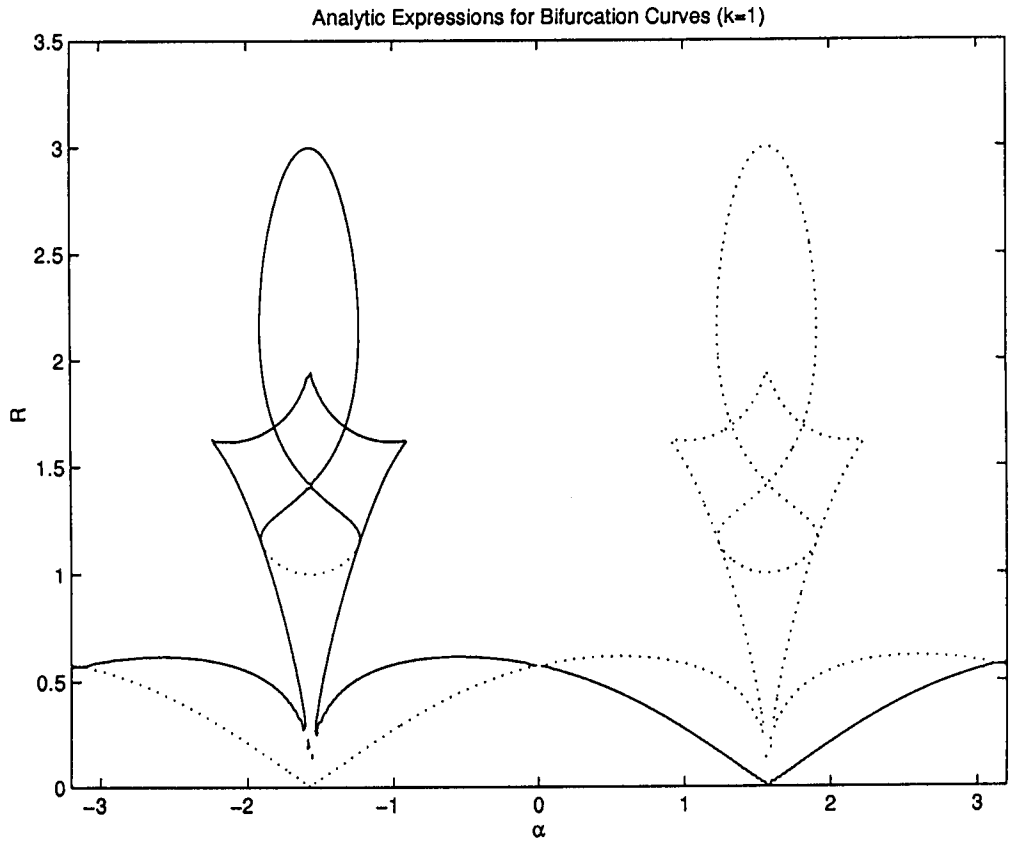

Fig.6. Bifurcation curves for $k = 1$, as obtained analytically. Dotted lines correspond to extraneous curve segments which were not present in the AUTO results.

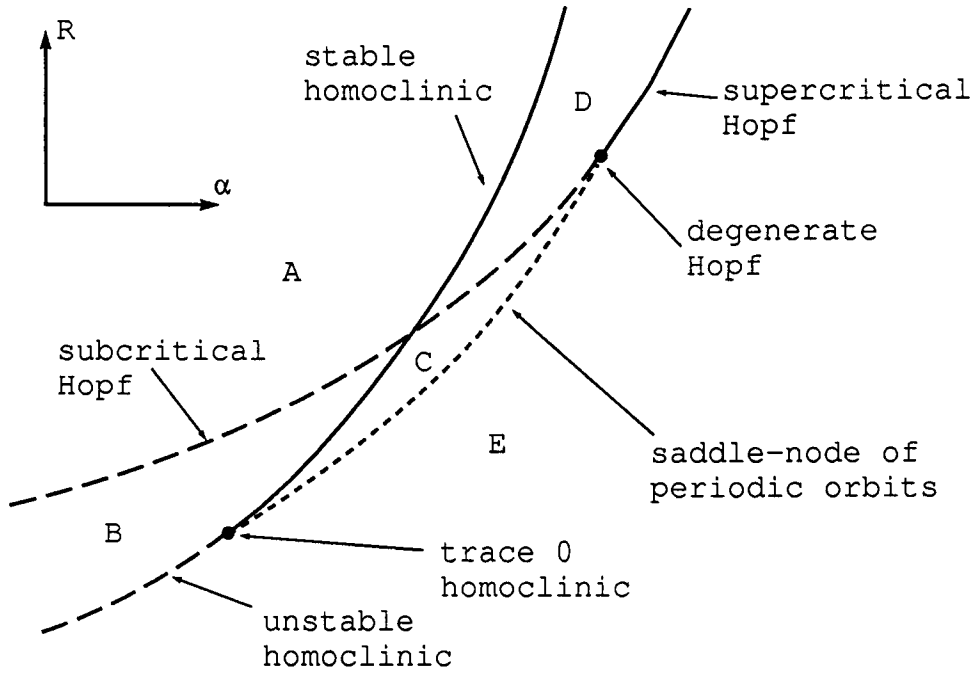

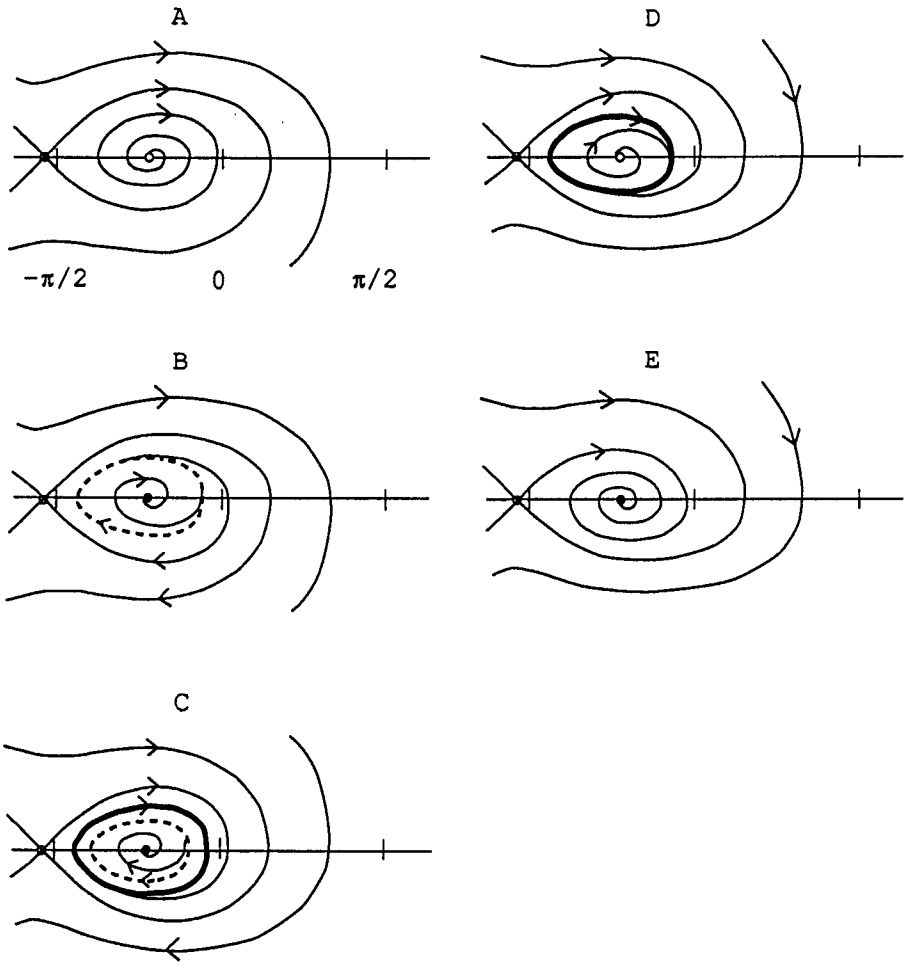

Fig.7. Crossing of Hopf and homoclinic bifurcation curves.

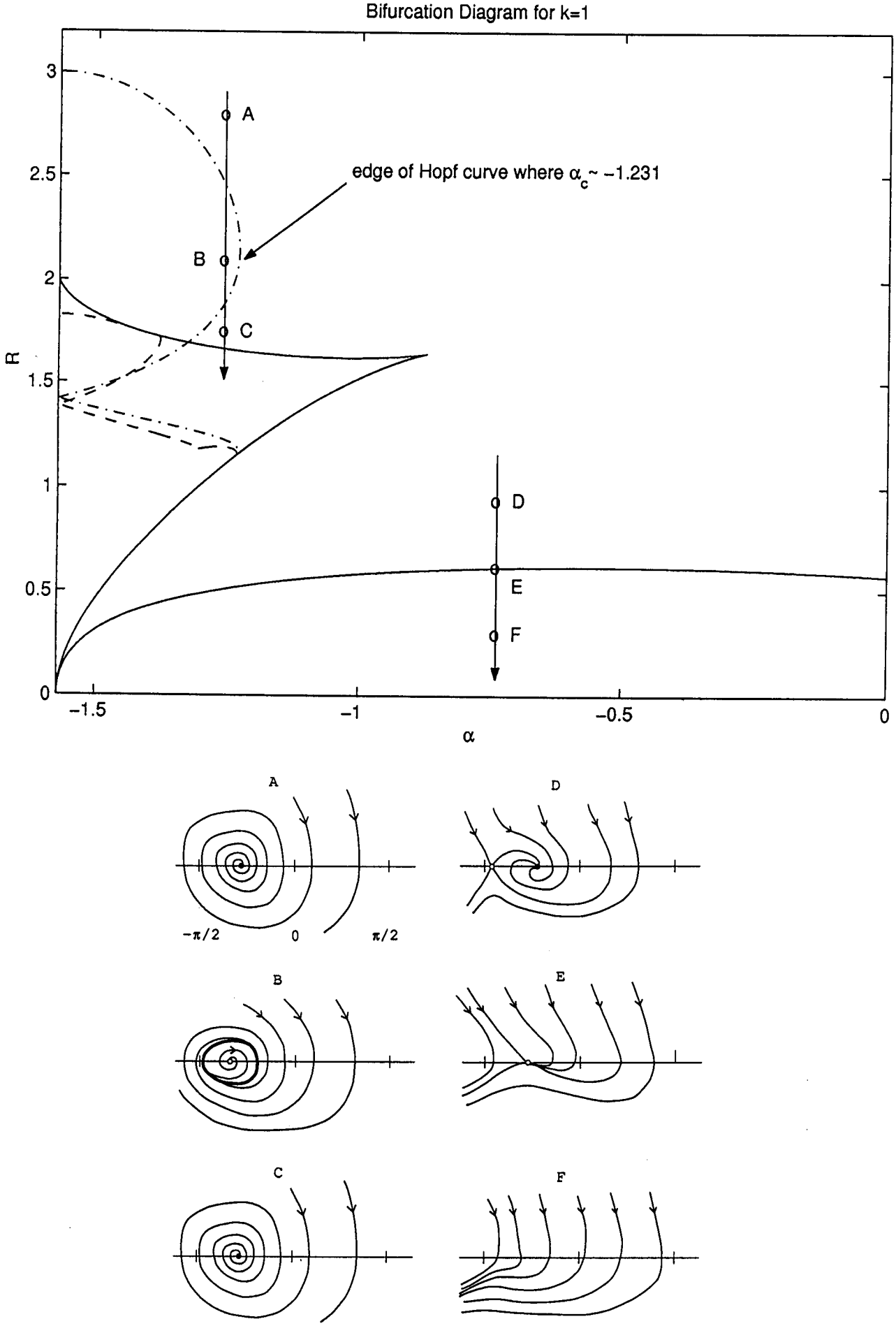

Fig.8. Phase portraits for $k = 1$.